Solid State Ionics 181 (2010) 551–556

Contents lists available at ScienceDirect

Solid State Ionics

journal homepage: www.elsevier.com/locate/ssi

A critical assessment of interatomic potentials for ceria with application to its elastic properties

Haixuan Xu (徐海譞), Rakesh K. Behera, Yanli Wang (王艳丽) [1], Fereshteh Ebrahimi, Susan B. Sinnott, Eric D. Wachsman, Simon R. Phillpot *

Department of Materials Science and Engineering, University of Florida, Gainesville, FL 32611, United States

ARTICLE INFO

Article history:
Received 9 April 2009
Received in revised form 26 January 2010
Accepted 18 February 2010

Keywords:
Ceria
Solid-oxide fuel cell
Mechanical properties
Elastic properties
Simulation
Molecular dynamics
Interatomic potentials

ABSTRACT

We critically assess the materials fidelity of six interatomic potentials for ceria, based on predicted lattice constants, thermal expansion, chemical expansion, dielectric properties, oxygen migration energy and mechanical properties. While, no potential can reproduce all fundamental properties, the Gotte (2007) and Grimes potentials display the combination of highest fidelity with the widest range of applicability. The simulations show that sub-stoichiometry leads to a significant softening of the elastic constant, which is consistent with the experimental results. Similar results are observed for doped-ceria systems.

1. Introduction

The industry standard electrolyte for solid-oxide fuel cells (SOFCs) is yttria-stabilized zirconia (YSZ) [1,2]. However, it suffers from the significant drawback that high temperature operation is required in order to produce oxygen ion mobility fast enough to support a significant current. Ceria-based materials [2–4] are being considered as a replacement for YSZ because the much higher conductivity of doped ceria compared to YSZ enables efficient operation at much lower temperatures.

A key issue for all putative electrolytes is mechanical stability. Recently some of us have characterized the elastic properties of both pure ceria and gadolinia doped ceria (GDC) [5] and found that the materials show significant elastic softening as the oxygen partial pressure decreased, i.e., as ceria becomes more sub-stoichiometric and GDC contains more oxygen vacancies. These results were interpreted using an analytic defect-equilibrium model [6].

In this paper, we address the issue of the mechanical properties of ceria and doped ceria using atomic-level simulation methods. Atomic-level simulation, molecular dynamics (MD) in particular, neatly complements the experimental and analytical approaches in that we can specify the composition of a system with atomic precision, and characterize the structure at the atomic level. The quantitative reliability of an MD simulation is determined by the materials fidelity of the interatomic potential used. There are a number of interatomic potentials for ceria in the literature. We therefore perform a survey of fundamental properties predicted using these potentials, which allows us to identify the potential(s) most suitable for the simulation of the effects of temperature and chemistry on the elastic properties. Using the most suitable potentials, our results are consistent with the experimental results in that the simulations show that sub-stoichiometry leads to a significant softening of the elastic constants. The effects of temperature and sub-stoichiometry on mechanical properties are investigated. We also find a similar degree of elastic softening in doped-ceria systems.

2. Simulation methodology

The lattice-statics and MD simulations carried out here use conventional simulation approaches. The overall ionic interactions are described as the sum of long-range and short-range contributions. The long-range interactions between different ionic species are described by a simple Coulombic interaction:

$$E_{LR}\left(r_{ij}\right) = \frac{1}{2}\sum_{i=1}^{N}\left\{\sum_{j\neq i}\frac{q_i q_j}{r_{ij}}\right\} \quad (1)$$

where N is the total number of ions in the system, q_i and q_j are the charge on ion i and j respectively, r_{ij} is the distance between ion i and j.

* Corresponding author. 162 Rhines Hall, MSE, University of Florida, Gainesville, FL – 32611-6400, United States. Tel.: +1 352 846 3782; fax: +1 352 846 3355.
E-mail address: sphil@mse.ufl.edu (S.R. Phillpot).
[1] Current address: Oak Ridge National Laboratory, Oak Ridge, TN 37831, United States.

0167-2738/$ – see front matter © 2010 Elsevier B.V. All rights reserved.
doi:10.1016/j.ssi.2010.02.023

The summations are carried out using the Ewald method. All of the potentials use the formal ionic charge for q (i.e., $q_{Ce}=+4$ and $q_O=-2$).

The most common functional form for the short-ranged interactions is given by the Buckingham form:

$$E_{Buck}\left(r_{ij}\right) = Ae^{\left(-r_{ij}/\rho\right)} - C/r_{ij}^6 \quad (2)$$

where A, ρ and C are adjustable parameters, chosen to reproduce pertinent physical properties of the real material.

Also commonly used is the Born–Mayer–Huggins (BMH) form:

$$E_{BMH}\left(r_{ij}\right) = f_0\left(b_i + b_j\right)\exp\left\{\left(a_i + a_j - r_{ij}\right)/\left(b_i + b_j\right)\right\} - c_i c_j / r_{ij}^6. \quad (3)$$

Here a_i, b_i and c_i are the parameters for individual atom species. Although the BMH form can be simply recast into the Buckingham form, it does have the advantage that, at least in principle, parameters for individual ions can be defined, rather than for ion pairs as in the Buckingham form. For ceria-based systems, potentials using both the Buckingham and BMH forms have been developed. Since the quality of the simulations is directly determined by the quality of the potential, an evaluation of the available potentials is given in Section 3.

The calculations used in the evaluation of the potentials are carried out using GULP (General Utility Lattice Program) [7,8]. All simulations are performed on a $6\times6\times6$ supercell of cubic non-primitive fluorite unit cells, each of which contains four CeO_2 formula units, for a total of 2592 ions. Periodic boundary conditions are applied in all three spatial directions. To simulate sub-stoichiometry, Ce^{4+} ions are randomly replaced by Ce^{3+} ($q=+3$) ions. Within a single simulation the arrangement of Ce^{4+} and Ce^{3+} ions is fixed; this is a limitation of the current approach, since experimentally electron transfer allows the Ce^{3+} ions to develop an equilibrium arrangement, which may not be random. An appropriate number of oxygen ions are then removed to maintain charge neutrality. Computational annealing of the system by MD at high temperature allows the oxygen vacancies to diffuse to form a structure in which the anion and vacancy arrangements are in equilibrium with respect to the fixed cation sublattice. For sub-stoichiometric ceria and doped ceria, since the properties may depend on the arrangements of dopant cations and oxygen vacancies, several random cation structures are generated and the properties of each structure are calculated to capture the range of effects. For the $T>0$ K calculations, the free energy is calculated using the quasi-harmonic approximation to lattice dynamics, as implemented in the GULP code.

Table 2
Parameters of Inaba [26] Born–Huggins–Mayer potential for CeO_2. No shell model is available for this potential.

		z	a (Å)	b (Å)	c ($J^{0.5}(nm)^3\ mol^{-0.5}$)
Inaba	Ce^{4+}	2.700	1.33	0.0454	0.00
	O^{2-}	−1.350	1.847	0.166	1.294

3. Potential evaluation

There are five different parameterizations of the Buckingham potentials and one parameterization of the BMH potential available for the ceria-based systems. The parameters for the five Buckingham potentials, denoted as Grimes [9], Vyas [10], Butler [11], Gotte (2004) [12], and Gotte (2007) [30], are given in Table 1. The Grimes, Gotte (2004) and Gotte (2007) potentials have also been parameterized for Ce^{3+}, allowing the effects of off-stoichiometry to be assessed. In addition, the Grimes potential has been parameterized for a number of rare-earth ions, allowing doping effects to be determined. The parameters for Inaba's BMH potential are given in Table 2. All of the Buckingham potentials have shell-model parameters; unless otherwise indicated all of the simulation results for these systems are based on shell-model calculations. In the shell model [13], each ion is considered to be composed of a core and a shell. The total charge on each ion is the sum of the respective core and shell charges (Y_e). The core and shell of each ion interact with those of other ions via long-ranged Coulombic interactions. There is also a short-range shell–shell interaction, which takes into account the repulsion between electron clouds of the atoms. The shell model mimics the presence of the nucleus plus core electrons (core) and valence electrons (shell). For any given atom, the core and shell are coupled by a spring constant (K_1). Inaba's BMH potential is a rigid-ion potential. To evaluate the quality of each potential, the lattice constant, thermal expansion, chemical expansion, oxygen migration energy, dielectric properties and mechanical properties are determined. The detailed comparison for these properties is given in the following subsections.

3.1. Lattice constant and thermal expansion

The zero-temperature lattice constants calculated using these potentials are listed in Table 3. The values are all essentially identical and in excellent agreement with the experimental data. This is to be expected since the potentials were fitted to the lattice parameter and some other fundamental properties. However, it should be noted that the experimental data is 293 K while simulation data are for 0 K.

Table 1
Parameters of the five Buckingham potentials for CeO_2. All are formal charge models.

	Species	A (eV)	r (Å)	C (eV Å ^{6})	Y_e (e)	K_1 (eV $Å^{-2}$)	Ref
Grimes	O^{2-}–O^{2-}	9547.96	0.2192	32.0	−2.04	6.3	[27]
	Ce^{4+}–O^{2-}	1809.68	0.3547	20.40	−0.20	177.84	[10]
	Ce^{3+}–O^{2-}	2010.18	0.3449	23.11			[22]
	In^{3+}–O^{2-}	1495.65	0.3327	4.33			[28]
	Y^{3+}–O^{2-}	1766.40	0.33849	19.43			[27]
	Gd^{3+}–O^{2-}	1885.75	0.3399	20.34			[22]
	La^{3+}–O^{2-}	2088.79	0.3460	23.25			[22]
Vyas	O^{2-}–O^{2-}	9547.92	0.2192	32.0	−2.04	10.3	[10]
	Ce^{4+}–O^{2-}	2531.5	0.335	20.40	−0.20	177.84	
Butler	O^{2-}–O^{2-}	22,764.3	0.149	45.83	−6.10	419.9	[11]
	Ce^{4+}–O^{2-}	1986.8	0.3511	20.40	7.7	291.8	
Gotte (2004)	O^{2-}–O^{2-}	9547.92	0.2192	32.0	60.78	−3.0	[12]
	Ce^{4+}–O^{2-}	1809.68	0.3547	24.40	166.021	7.0	
	Ce^{3+}–O^{2-}	1809.68	0.3547	24.40	166.021	7.0	
Gotte (2007)	O^{2-}–O^{2-}	9533.421	0.234	224.88	1759.8	−6.5667	[29]
	Ce^{4+}–O^{2-}	755.1311	0.429	0.0	43.451	4.6475	
	Ce^{3+}–O^{2-}	1140.193	0.386	0.0	2172.5	15.092	

Table 3
Properties of CeO_2 from experiment and from various interatomic potentials.

	Exp.	Empirical potential					
		Grimes [22]	Vyas [10]	Butler [11]	Gotte (2004) [12]	Gotte (2007) [29]	Inaba [26]
Lattice constant (Å)	5.411	5.411	5.414	5.411	5.411	5.411	5.414
Coefficient of thermal expansion ($\times 10^{-6}$ K^{-1})	11.6	1.27	1.16	13.1	6.65	7.31	9.58
Coefficient of chemical expansion at 1173 K (Å/oxygen vacancy concentration)	0.535	0.41	–	–	0.505	0.43	–
Static relative permittivity	18.6–20.0	18.6	12.71	19.53	16.2	18.6	–
High frequency dielectric	4	4.54	3.98	4	5.59	4	
Oxygen migration energy (eV)	0.7 ± 0.1	0.3 (shell model) 0.63* (rigid ion)	0.54	0.74	0.41 (shell model) 0.58* (rigid ion)	0.58	0.54

Chemical expansion is calculated at 1173 K. * indicate value without shell model.

To determine the thermal expansion, the temperature dependence of the lattice parameter for each potential (normalized to the corresponding $T = 0$ K values) is shown in Fig. 1. The quasi-harmonic approximation used for these calculations includes quantum effects, which leads to zero thermal expansion at $T = 0$ K. The coefficient of thermal expansion values given in Table 3 is taken from $T = 400$ K to $T = 1400$ K over which the lattice parameter is approximately linear in temperature and over which quantum effects are no longer important.

None of these potentials is able to quantitatively reproduce the experimental value. It is found that the Butler potential overestimates the experimental thermal expansion, whereas the others underestimate the thermal expansion. The thermal expansion calculated by the Butler and Inaba potentials, which are 112% and 82% of the experimental value, are better than the other values. The thermal expansion calculated using Gotte (2007), Gotte (2004), Vyas and Grimes potentials predict values that are 63%, 57%, 10% and 11% of the experimental value, respectively.

3.2. Chemical expansion

The chemical expansion measures the lattice expansion produced by off-stoichiometry. To simulate this, we introduce oxygen vacancies into the pure ceria system and replace the requisite number of Ce^{4+} ions with Ce^{3+} ions. The effect of this sub-stoichiometry on the lattice parameter is four-fold: (i) the larger ionic radius of the Ce^{3+} compared to the Ce^{4+} ions (1.143 Å vs. 0.97 Å) tends to increase the lattice parameter; (ii) the lower charge of the Ce^{3+} reduces the strength of the attractive Coulombic interactions, thereby also tending to increase the lattice parameter; (iii) the presence of oxygen vacancies decreases the attractive Coulombic interactions, also tending to an increased lattice parameter; and (iv) the oxygen vacancies also have the effect of lowering the atomic density, thereby tending to decrease the lattice parameter. We note that three of these four effects can be expected to lead to an increase in the lattice parameter with increasing sub-stoichiometry.

As mentioned above only three of the potentials have parameters for Ce^{3+}: Grimes, Gotte (2004) and Gotte (2007). Fig. 2 compares the simulated lattice parameters at 1073 K using the Grimes, Gotte (2004) and Gotte (2007) potentials with the experimental value for CeO_{2-x} ($x = 0.0$–0.15) [14,15]. The simulation results (solid symbols) show that the lattice parameters increase with increasing vacancy concentrations, consistent with the qualitative argument above. The slope of the chemical expansion line with respect to x in CeO_{2-x} is given in Table 3. It is found that both Grimes and Gotte (2007) potential give a chemical expansion close to the experimental results, which indicates that both potentials successfully capture the effects of sub-stoichiometry.

3.3. Dielectric properties and oxygen migration energies

As shown in Table 3, most of the potentials yield static and high frequency dielectric constants within ~10% of the experimental values. The exception is the Gotte (2004) potential, which overestimates the dielectric constant by ~40%. The oxygen migration energy predicted by Grimes and Gotte (2004) is significantly smaller than the experimental value. Interestingly, using the Grimes potential in the rigid-ion approximation, rather than with a shell model, the predicted oxygen migration energy is in excellent agreement with the experimental results. The Gotte (2004) potential also predicts higher migration

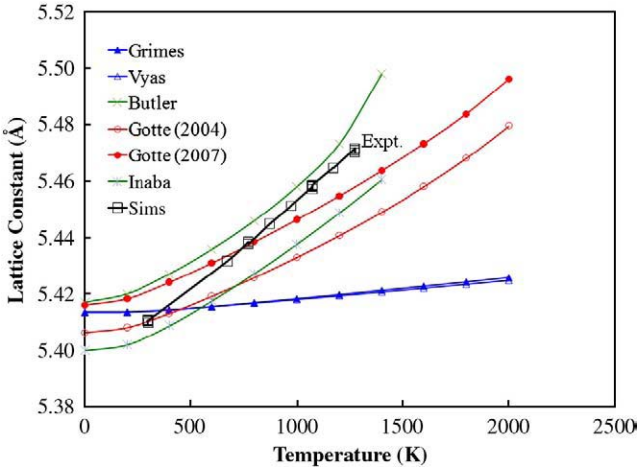

Fig. 1. Temperature dependence of the lattice parameter of CeO_2 obtained from MD simulation using different potentials, compared with the experimental data [32].

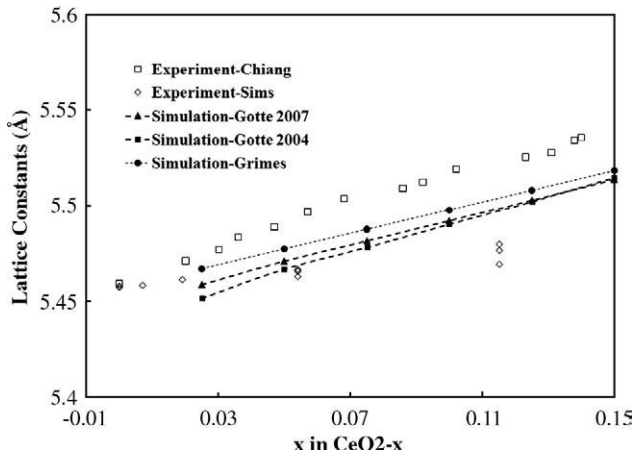

Fig. 2. The effect of composition on the lattice parameter of CeO_{2-x} obtained from MD simulation at 1073 K. The values are compared with the experimental results [14,32].

energy when the shell model is not used. Physically, this is quite reasonable since the polarizability of the ions in the shell model allows charges of the ions to polarize in a manner that lowers the energy barriers. The oxygen migration energy calculated using Vyas, Butler, Gotte (2007) and Inaba is in reasonably good agreement with the experimental data.

3.4. Elastic properties

Table 4 compares the zero-temperature elastic constants, as determined directly from GULP for the various potentials, with the experimental results and with DFT.

Experimental values for the elastic properties are also given in Table 4. The values of C_{11}, C_{12} and C_{44} were obtained from Raman scattering, which probes the fundamental vibrations of the system [16]. The value of the bulk modulus determined from these values is in quite good agreement with independent determinations from pressure–volume curves [17]. Likewise, the Young's modulus obtained from analysis of the Raman scattering results is in good agreement with the value from nanoindentation [5].

For the simulations, the values of C_{11}, C_{12} and C_{44} were determined in GULP, from which all of the moduli and the Z parameter were determined using standard analytic elastic relationships. The values predicted by the Grimes, Vyas, Butler, Inaba and Gotte (2004) potentials are all larger than the corresponding experimental values. The values obtained for the Gotte (2007) are in perfect agreement with the experimental values. Although not discussed in their paper, it can reasonably be assumed that the experimental elastic properties were part of the fitting set for the potential. The bulk modulus, B, tetragonal shear modulus, G, and Young's modulus, Y, show corresponding levels of agreement with the experiment.

Also included in this table are the results of previous electronic-structure calculations [31] at the level density functional theory (DFT) using the local density approximation (LDA) with the projector augmented wave (PAW) method [18].

Both the atomistic simulations and the electronic-structure calculations were performed on ideal crystals. We therefore used the Voigt–Reuss–Hess method [19] to determine polycrystalline-average elastic constants from the single-crystal values. Because $C_{11} = C_{33}$ and $C_{12} = C_{13} = C_{23}$ for a cubic system, the polycrystalline average of the bulk modulus is identical to the single crystal value. The Hess average is shown in Table 4.

The polycrystalline averaged shear modulus lies within the bounds [19]:

$$G_R = \frac{5(C_{11}-C_{12}) \times C_{44}}{4C_{44} + 3(C_{11}-C_{12})} < G < G_v = \frac{C_{11}-C_{12} + 3C_{44}}{5}. \quad (4)$$

The elastic anisotropy of the material can be characterized by the directionality of the Young's modulus, E, can also be determined using:

$$E^{-1} = \frac{C_{11} + C_{12}}{(C_{11}-C_{12})(C_{11} + 2C_{12})} - C_{44}[Z-1]\left[\sin^2\theta\cos^2\theta + \frac{1}{4}\sin^4\theta\sin^2 2\Phi\right] \quad (5)$$

where θ is the angle between [100] axis and the chosen direction and Φ is the angle between [010] axis and the projection of the chosen direction on the (100) plane. Here Z is the Zener anisotropy ratio:

$$Z = \frac{2C_{44}}{C_{11}-C_{12}}. \quad (6)$$

For $Z = 1$, the system is isotropic, and the Young's modulus is independent of direction.

Since all of these metrics of the elastic properties were determined analytically from the elastic constants, they show corresponding degrees of agreement with the experimental values.

3.5. Potential summary

None of the potentials is able to reproduce all of the experimental properties evaluated. Overall, the Gotte (2007) has the highest materials fidelity. In particular, the elastic and dielectric properties are in essentially perfect agreement with the experiment, and the predicted oxygen migration energy is in good agreement with the experiment. The chemical expansion is also in reasonable agreement with the experimental data. However, the predicted thermal expansion is smaller than the experimental value, indicating that the potential is significantly less anharmonic than the experimental system.

Interestingly, the Grimes potential predicts the chemical expansion to within 20%. It also yields dielectric properties and the oxygen migration energy in good agreement with the experiment. However, it cannot reproduce thermal expansion, predicting a value that is only 11% of the experimental value. In terms of the elastic properties, the Grimes potential is clearly not as good as the Gotte (2007) or Inaba potentials, but has a similar level of fidelity as the other potentials. To its advantage, the Grimes potential is the only potential providing parameters for some rare-earth ions, which allows the study of doped-ceria system.

In the next section, we evaluate the effects of off-stoichiometry on the elastic properties. Because both the Grimes and Gotte (2007) potentials do predict some of the salient properties with reasonable accuracy, we will compare the results predicted for each. In Section 5,

Table 4
Comparison of elastic properties, including the bulk modulus, B, Young's modulus, Y, and shear modulus, $G = 1/2\ (C_{11}-C_{12})$, of CeO_2 from experiment, DFT calculations and as predicted by empirical potentials. Those experimental and simulated values that were independently determined are given in bold. Others were determined using standard relationships among elastic properties.

	Exp.	Buckingham					BMH	DFT
	All units in GPa	Grimes [22]	Vyas [10]	Butler [11]	Gotte (2004) [12]	Gotte (2007) [29]	Inaba [26]	
C_{11}	**403.0** [16]	**554.2**	**573.0**	**504.4**	**554.0**	**403.0**	**451.0**	**399.5** [30]
C_{12}	**105.0** [16]	**124.6**	**147.7**	**143.1**	**125.0**	**105.0**	**103.6**	**127.5** [30]
C_{44}	**60.0** [16]	**123.6**	**146.8**	**16.1**	**71.7**	**60.0**	**99.1**	**63.5** [30]
B	204 **236 ± 4** [17] **230 ± 10** [31]	267.9	289.4	263.6	268.0	204.3	207.0	218
G	149.0	215.0	212.6	180.7	214.5	149.0	173.7	136
Y	–	508.0	512.5	439.7	511.2	362.4	412.3	338
G_{Poly}	96.0	160.2	173.4	81.8	128.2	96.0	124.3	92.5
Y_{Poly}	248.95 **255** [5]	400.7	433.6	222.4	331.7	249.0	310.6	243.1
Z	0.40	0.58	0.69	0.09	0.33	0.40	0.57	0.46

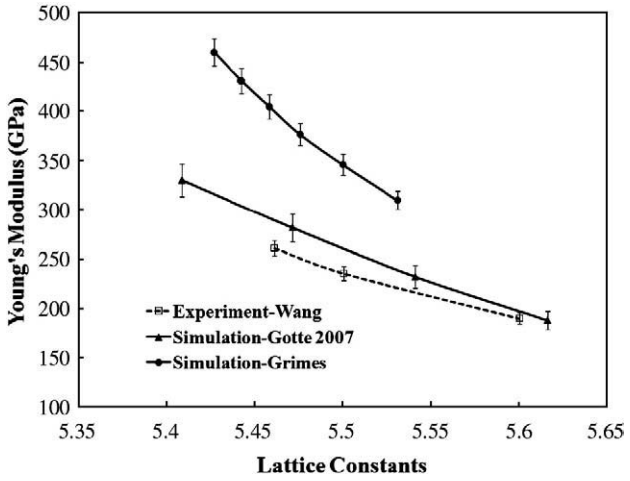

Fig. 3. Composition dependence on the room temperature Young's modulus of CeO_{2-x} obtained from MD simulation using Gotte (2007) potential, Grimes potential and from experiment.

we examine the effects of rare-earth doping on the elastic properties, for which the Grimes potential is the only one with potential parameters.

4. Elastic properties of CeO_{2-x}

A key finding in the experimental measurements of Wang et al. [5] for the Young's modulus of ceria was that there is significant elastic softening with decreasing oxygen partial pressure (P_{O2}), i.e., with increasing sub-stoichiometry [5]. The open symbols in Fig. 3 denote the room temperature Young's modulus for the different levels of sub-stoichiometry, determined from their data. The experiments were actually performed at fixed P_{O2}, at which the lattice parameter was determined. The corresponding degree of off-stoichiometry can be calculated from the method developed by Bevan and Kordis [20] and Panlener et al. [21]. Fig. 3 also shows the corresponding results predicted from the Grimes and Gotte (2007) potentials at 300 K. In Fig. 3, the Young's moduli are plotted as a function of lattice constants rather than of the composition. There are differences between the predicted chemical expansions and the experimental value; it thus turns out that the direct calculated Young's moduli agree with the experimental values quite well for the Gotte (2007) potential. The Grimes potential agrees less well, mainly due to the significant overestimate in the elastic constant of the pure system.

In contrast to the Raman scattering experiments, the DFT calculations and MD simulations (Table 6), the nanoindentation experiments of Wang et al. [5] did not show significant elastic anisotropy. It is possible that microstructural factor in the indented samples leads to effectively isotropic elastic behavior, rather than the anisotropic behavior seen in the spectroscopy experiments [16], which probe the intrinsic atomic-level elastic response.

We have also used atomic simulations to determine the effect of temperature on the elastic properties of CeO_2 using the Gotte (2007) potential, which has the highest fidelity in elastic properties for ceria system. Fig. 4 shows the temperature dependence of Young's modulus (Y) in the <001> direction, the shear modulus (G), the bulk modulus (B), and the anisotropy factor. The trends are in accord with conventional trends for the softening of the elastic properties with temperature. The elastic anisotropy factor also decreases with increasing temperature.

Table 5
Ionic radii for relevant ions from Shannon table [24].

	Ionic radius (VIII)
Ce^{4+}	0.97 Å
In^{3+}	0.92 Å
Y^{3+}	1.019 Å
Gd^{3+}	1.053 Å
Ce^{3+}	1.143 Å
La^{3+}	1.16 Å

5. Mechanical properties of $Ce_{1-2x}M_{2x}O_{2-x}$

We have determined the effects of doping of ceria doped with In^{3+}, Y^{3+}, Gd^{3+}, and La^{3+} ions, for which the potential parameters compatible with the Grimes potential were provided by Minervini et al. [22]. The ionic radii of these dopant ions are given in Table 5. The Grimes potential fails to accurately predict the thermal expansion and oxygen migration energy. However, the most two important properties for addressing the effects of doping are the chemical expansion, for which its description is reasonable, (Fig. 2) and the elastic constants (Table 4), for which it captures the trends, albeit being overall too stiff.

We compare the lattice constants of various doped-ceria systems with the experimental values. In a manner analogous to that for CeO_{2-x}, the doped structures are generated by randomly replacing the Ce^{4+} ions by dopant cations and compensating the charge by creating appropriate number of oxygen vacancies in the system.

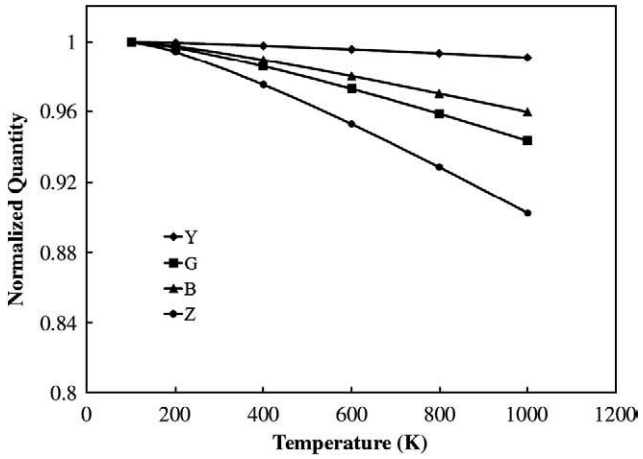

Fig. 4. The effects of temperature on the normalized bulk modulus, shear modulus, and Young's modulus for CeO_2, as determined by MD simulation using Gotte (2007) potential.

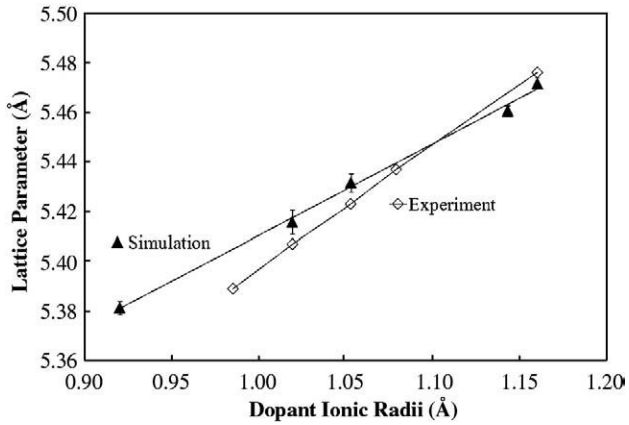

Fig. 5. The effect of dopant ion size on the lattice parameter of $Ce_{0.8}M_{0.2}O_{1.9}$ (where $M = In^{3+}$, Y^{3+}, Gd^{3+}, Ce^{3+}, La^{3+}) obtained from MD simulation, compared with the experimental results [23].

Table 6
Anisotropy in the Young's modulus of CeO_2 using different methods. Numbers in brackets indicate value relative to that in the <001> direction.

Directions	Grimes [22]	Gotte (2007) [29]	DFT [30]	Exp.
<0 0 1>	504.9 (1.0)	359.6 (1.0)	355.9 (1.0)	359.6 (1.0)
<1 1 0>	351.6 (0.70)	189.8 (0.53)	196.7 (0.55)	189.8 (0.53)
<1 1 1>	319.3 (0.63)	163.9 (0.46)	171.2 (0.48)	163.9 (0.46)

Since the experimental results for dopants are already available at 298 K and the effect is more pronounced for a larger dopant concentration, room temperature $Ce_{0.8}M_{0.2}O_{1.9}$ was simulated, where $M = In^{3+}$, Y^{3+}, Gd^{3+}, and La^{3+} ions. Fig. 5 compares the simulated lattice parameters using the Grimes potential with the experimental values [23]. The simulated values are within 0.2 Å of the experimental values over the full range of ionic radii [24], which can be considered to be adequate agreement. As is evident from Fig. 5, the simulations show a consistently weaker dependence of the lattice parameter on the ionic radius of the dopant ion. This is consistent with the calculated lower chemical expansion in CeO_{2-x} (see Table 3).

For fuel-cell electrolyte applications, it is also important to understand the effect of dopants on the Young's modulus of doped-ceria system. From the point of view of the atomic-level simulation, the approach is essentially identical to that for sub-stoichiometric CeO_2 since the Ce^{3+} ions and M^{3+} ions act in the same manner. Experimentally, the Young's modulus of $Ce_{0.8}Gd_{0.2}O_{1.9}$ at room temperature is determined to be 147.2 ± 16.1 GPa [25], whereas the Grimes potential predicts twice this value. As previously discussed, the Grimes potential overestimates the Young's modulus of pure and reduced ceria system by similar amounts. However, the relative trend of Young's modulus dependence on ionic radii should be more reliable than the absolute value. As Fig. 6 shows, the system becomes elastically softer with increasing ionic radius of the dopant. Similar elastic softening effects have been observed experimentally in doped-ceria systems [5].

6. Discussion

The materials fidelity of six different empirical potentials has been evaluated, based on lattice constant, thermal expansion, chemical expansion, dielectric properties, oxygen migration energy and mechanical properties. No single potential can reproduce all fundamental properties. Therefore, choosing the appropriate potential(s) for specific application is critical. In general, the Gotte (2007) has the highest overall fidelity, while the Grimes can be applied to the widest range of systems.

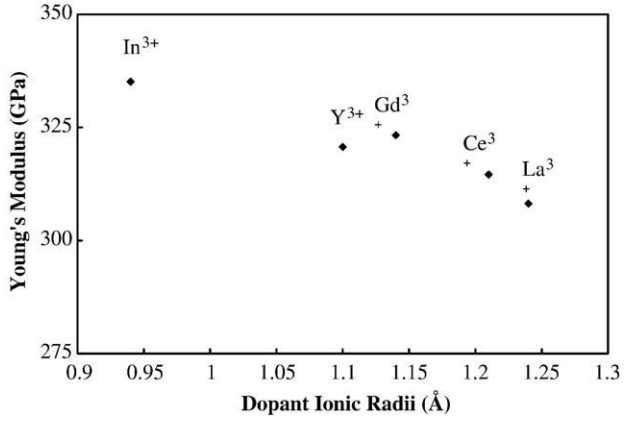

Fig. 6. Dopant size dependence on the Young's modulus of $Ce_{0.8}M_{0.2}O_{1.9}$ (where M = In^{3+}, Y^{3+}, Gd^{3+}, Ce^{3+}, La^{3+}) obtained using Grimes potential.

The simulations, using the best available potential(s) for each physical property, show that both sub-stoichiometry and aliovalent doping of ceria lead to large decreases in the elastic constants of the material. These decreases arise from the significantly reduced strength of ionic interactions. If this elastic softening were to be so large as to threaten the mechanical integrity of the system, then it would pose a challenging problem for the design of ceria-based electrolytes. It appears that the only way to mitigate this softening would be to strengthen the ionic interactions in the system. Of course, reducing the amount of doping or the sub-stoichiometry would do this; however it would also significantly reduce the ionic conductivity of the system, which is the key performance metric of the material. It would thus be of significant value to identify a strategy for increasing the ionic conductivity that does not result in a significant softening in the elastic properties.

Acknowledgements

This work was supported by NASA under the grant NAG3-2930 and by DOE through the High Temperature Electrochemistry Center at the University of Florida, Contract No. DE-AC05-76RL01830.

References

[1] S.P.S. Badwal, Solid State Ionics 52 (1992) 23.
[2] T.H. Etsell, S.N. Flengas, Chemical Reviews 70 (1970) 339.
[3] M. Mogensen, N.M. Sammes, G.A. Tompsett, Solid State Ionics 129 (2000) 63.
[4] V.V. Kharton, F.M.B. Marques, A. Atkinson, Solid State Ionics 174 (2004) 135.
[5] Y.L. Wang, K. Duncan, E.D. Wachsman, F. Ebrahimi, Solid State Ionics 178 (2007) 53.
[6] K.L. Duncan, Y.L. Wang, S.R. Bishop, F. Ebrahimi, E.D. Wachsman, Journal of Applied Physics 101 (2007) 044906.
[7] J.D. Gale, Journal of the Chemical Society-Faraday Transactions 93 (1997) 629.
[8] J.D. Gale, A.L. Rohl, Molecular Simulation 29 (2003) 291.
[9] R.W. Grimes, G. Busker, M.A. McCoy, A. Chroneos, J.A. Kilner, S.P. Chen, Berichte Der Bunsen-Gesellschaft-Physical Chemistry Chemical Physics 101 (1997) 1204.
[10] S. Vyas, R.W. Grimes, D.H. Gay, A.L. Rohl, Journal of the Chemical Society-Faraday Transactions 94 (1998) 427.
[11] V. Butler, C.R.A. Catlow, B.E.F. Fender, J.H. Harding, Solid State Ionics 8 (1983) 109.
[12] A. Gotte, K. Hermansson, M. Baudin, Surface Science 552 (2004) 273.
[13] B.G. Dick, A.W. Overhauser, Physical Review 112 (1958) 90.
[14] H.W. Chiang, R.N. Blumenthal, R.A. Fournelle, Solid State Ionics 66 (1993) 85.
[15] J.R. Sims, R.N. Blumenthal, High Temperature Science 8 (1976) 99.
[16] A. Nakajima, A. Yoshihara, M. Ishigame, Physical Review B 50 (1994) 13297.
[17] L. Gerward, J.S. Olsen, L. Petit, G. Vaitheeswaran, V. Kanchana, A. Svane, Journal of Alloys and Compounds 400 (2005) 56.
[18] R.M. Martin, Electronic Structure: Basic Theory and Practical Methods, Cambridge University Press, New York, USA, 2004.
[19] D.J. Green, An Introduction to the Mechanical Properties of Ceramics, Cambridge University Press, 2004.
[20] D.J.M. Bevan, J. Kordis, Journal of Inorganic & Nuclear Chemistry 26 (1964) 1509.
[21] R.J. Panlener, R.N. Blumenthal, J.E. Garnier, Journal of Physics and Chemistry of Solids 36 (1975) 1213.
[22] L. Minervini, M.O. Zacate, R.W. Grimes, Solid State Ionics 116 (1999) 339.
[23] S. Sameshima, H. Ono, K. Higashi, K. Sonoda, Y. Hirata, Y. Ikuma, Journal of the Ceramic Society of Japan 108 (1060) (2000).
[24] R.D. Shannon, Acta Crystallographica. Section A 32 (1976) 751.
[25] N. Sammes, G. Tompsett, Y.J. Zhang, A. Cartner, R. Torrens, Denki Kagaku 64 (1996) 674.
[26] H. Inaba, R. Sagawa, H. Hayashi, K. Kawamura, Solid State Ionics 122 (1999) 95.
[27] R.W. Grimes, G. Busker, M.A. McCoy, A. Chroneos, J.A. Kilner, S.P. Chen, Physical Chemistry Chemical Physics 101 (1997) 1204.
[28] M.A. McCoy, R.W. Grimes, W.E. Lee, Philosophical Magazine 76 (1997) 1187.
[29] A. Gotte, D. Spangberg, K. Hermansson, M. Baudin, Solid State Ionics 178 (2007) 1421.
[30] V. Kanchana, G. Vaitheeswaran, A. Svane, A. Delin, Journal of Physics-Condensed Matter 18 (2006) 9615.
[31] S.J. Duclos, Y.K. Vohra, A.L. Ruoff, A. Jayaraman, G.P. Espinosa, Physical Review B 38 (1988) 7755.
[32] J.R. Sims, R.N. Blumenthal, High Temperature Science (1976) 99.